# Simulation and Analysis of Variable Antenna Designs for Effective Stroke Detection

Amor Smida*
Department of Medical Equipment Technology, College of Applied Medical Sciences
Majmaah University, AlMajmaah 11952, Saudi Arabia
Microwave Electronics Research Laboratory, Department of Physics Faculty of Mathematical
Physical and Natural Sciences of Tunis, Tunis ElManar University, Tunis 2092, Tunisia

***Abstract*—The variety of applications of patch antenna for portable applications has opened the avenues for the possibilities of having compact, cost-efficient, and life-saving devices. Considering the challenges of portability and cost in making it feasible for detecting strokes in the masses of developing countries where the demand is quite high, this study builds the groundwork for such device fabrication. In total five antenna designs were investigated for their assessment in identifying the stroke. Two main studies of electromagnetic wave interaction and bio-heating of the human head phantom had been accomplished and the results are compared. The main comparison and identification of the stroke location with the human head phantom are presented by the specific absorption rate (SAR), both visualized as volumetric plot and stacked contour slices for clarifying the shape and positioning of the stroke in vertical and horizontal dimensions. The results show that the SAR values for Antenna A & D are the lowest with the values of 1.44 x 10-5 W/kg and 1.96 x 10-5 W/kg, respectively. But the induced electric field and isothermal temperature achieved were highest by Antenna D, with values of 0.25 emw and 133.92 x 10-8 K, respectively; and, the 2-D far-field radiation patterns confirmed better performance by it amongst all others. Hence, making the Antenna D as the most preferred choice for the prototyping stage. The overall trade-off of key parameters is studied herein in this simulation study and based on that the most suitable antenna design is proposed for the experimental prototype testing. The results suggest that the simulation results give a clear insight into the feasibility of stroke detection with the proposed setup and presents high viability for portable, low-cost, and rapid stroke detection applications.**

***Keywords*—Stroke detection; Specific Absorption Rate (SAR); Patch Antenna; S-parameter (S11); electromagnetic wave; bio-heat transfer***

## I. Introduction

In the past decade, the WHO declared cerebrovascular accidents (stroke) as the first reason for neurological dysfunction in the western world and based on worldwide statistics second most critical reason for mortality and the third rising reason for disability [1]. The sudden disruption of blood flow in some parts of the brain occurs due to a blockage or rupture that causes the death of brain cells and in the severe case may even lead to dementia and acute depression [2]. Every year globally almost 5 million people die and the other 5 million are rendered disable due to such stroke-related accidents. Though the major impact is seen on the low and middle-income group countries, wherein 70% of the total stroke cases are reported and 87% of the total deaths and disability-adjusted life years (DALYs viz. a term combining years spent with disability and years of life lost) occurs [3-5]. The disparity in the number of reported cases between the developing and developed countries is almost seven times [3].

Currently, the guidelines for stroke management are to undergo a series of treatments as per the resulting diagnosis. But there are relatively only two widely used methods available for stroke diagnosis i.e. X-ray based computer tomography (CT) and magnetic resonance imaging (MRI) [6]. Both are only available in the most advanced health centers and involve a huge cost of setup establishment, hence very scarcely available for the ongoing demand of diagnosis. Of which the MRI is even rarer due to its overall make complexity, cost and likewise the challenging operable skills demanded [7]. Even CT scans demand a greater skill for efficiently interpreting the results by a practicing professional, consequently creating delays or misinterpretations. And the adverse effects of X-ray make it even harder for continuous monitoring due to the limited safety exposure limits of these ionizing radiations [8]. If strokes can be identified at a very early stage, then accompanied by suitable remedial measures and prevention strategies the rate of stroke mortality can be effectively reduced [9, 10]. Moreover, the demand for effective, portable, and cost-effective system is the main research question currently that can address all the above-listed limitations away.

Considering the emerging demands stroke monitoring and detection have become a focus for developing more cost-effective and easily implementable techniques. Of which the Microwave Imaging (MWI) seems very promising due to its ease of setup and operation; with the capability to give a quick diagnosis as a complementary tool for the prehospital record on the type, size, shape, in some cases the number of blood blockages and as a harmless setup for continuous monitoring of the effect due to ongoing treatment since no harmful irradiations are involved herein [11-14]. MWI takes the concept of variable reflections from surfaces with different permittivity and conductivity and helps build a 3D mapping of the model under study. This concept is now explicitly applied for mapping the human head phantom with the idea to locate the stroke at early stages with clear visualization of its shape, size, and most importantly their numbers with each one's

*Corresponding Author

precise location. Many prototype devices are now been proposed and developed based on this concept [15-25]. Some are now even popularly applied as a commercial solution [18, 23, 24].

Since the effectiveness of the MWI is mainly dictated by the number and type of antennas employed involved the efforts for portable device development are mostly focused on tuning the involved parameters. In the lieu of getting improved results, there have been cases wherein almost 177 antenna arrays were tested for successful head model reconstruction and stroke identification [18]. Such expansive use of antennas imposes a serious challenge on the practical implementation of the model whilst prototyping and commercializing the concept. Hence, the need for a much powerful but lesser number of antenna involvement. The study herein proposes a concept for analyzing the human head phantom for stroke identification using an array of only 8 patch antennas, making it more viable for practical implementation. Though there are five different antenna designs studied for understanding the suitability of a design for its effectiveness in stroke identification. The simulation study presented herein compares the performance of each antenna design and gives clear practical reasoning for selecting one of them for future experimental studies. Also, the results clearly present the concept for generating 3D results for identifying the stroke shape, size, and location effectively. The combined analysis of the chosen antenna designs along with the 3D model concept for stroke identification makes this study different from the existing ones [16, 17, 20, 22, 25] and paves the way for streamlined laboratory testing with the best performing design.

In this paper, the concept of stroke identification and its location is presented along with an analysis of the antenna design most suitable to use. Among the five antennas it designed for 2.4 GHz band and lower SAR values and making them a favorable choice. Further, the antenna designs are also simulated to observe the effect on the reflection parameter/gain and the changes of SAR value with different designs.

## II. Numerical Setup

### A. Antenna Designs

For this study variable antenna designs were chosen for comparing their performances in terms of suitability for stroke identification, though considering the future manufacturing constraints not very intricate models were used. As it would be easy to make the intricate layouts and test them in simulation, but the next prototyping stage might face various issues and eventual delays due to limitations in manufacturing capability; in Fig. 1 The different antenna layout designs layouts with all the key dimensions of all the antenna designs studied. These were modeled separately in ProE CAD software to provide greater flexibility in designing the various dimensional aspects.

### B. Simulation Setup

The simulation is setup within the COMSOL Multiphysics 5.4 version software. The imported head phantom geometry used for this simulation study is recreated following the reference specific anthropomorphic mannequin (SAM) as mentioned in IEEE 1528 [26] and IEC 62209-1 [27]. It was developed by the IEEE Standards Coordinating Committee 34, Subcommittee 2, Working Group 1 (SCC34/SC2/WG1). It was chosen for this study since it is the widely used model for radiation related study on the human head and is followed by renowned organizations like the Association of Radio Industries and Businesses in Japan [28], European Committee for Electrotechnical Standardization (CENELEC) [29], the US Federal Communications Commission [30], etc. Though to reduce the problem size the model is scaled down by 60% with minor adjustments, to reduce the mesh complexity and save computational cost. Using the properties of cortical bone tissue within an ellipsoid geometry the simplified brain model was rendered to embody the human head phantom.

Further, each antenna design as described above was imported in COMSOL and was defined with materials as a layer of metal for the patch and FR4 dielectric material for the baseboard including ground. The metal patch was defined as a perfect electric conductor (PEC) having a negligible loss, within the radio frequency (RF) module's electromagnetic waves frequency domain interface. And the power source is represented by a lumped port fed by 50 Ω boundary condition. 8 x antennas in array form were arranged around the phantom at a radius of 130 mm. The stroke was modeled as a spherical (10 mm radius) mass of blood with the appropriate permittivity and conductivity values. To avoid unwanted reflection, the head phantom containing the stroke along with the antenna array were all enclosed within a perfectly matched layer (PML) spherical air domain. Which absorbs all outgoing waves, acting as an anechoic chamber and represented that the testing was done within infinite open space.

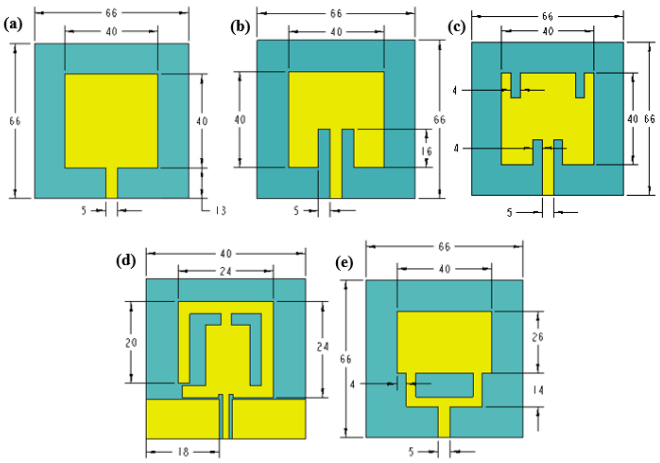


Fig. 1. The different Antenna Layout Designs Tested in this Simulation Study for the Human Head Stroke Detection by Potable Setup Application.

The analysis was carried out as two studies viz. bio-heating and electromagnetic (EM) wave interaction of the human head phantom. The volumetric interpolation model sampling function takes data from an MRI scan processed as an image data file with 109 slices and finally imported as a text file [31]. This text file relates the variation of tissue type within the created phantom model as to the real human head. And the exact material properties were taken from reference [32] which are summarized in Section 1 (S1) of Supporting Information. The patch antenna excited by lumped port emits the radiation which is directed onto the phantom by the array arrangement. The working frequency was chosen as 2.45 GHz as the general norm for on body and in body applications stated by industrial, scientific, and medical (ISM) bandwidth is in the range of 2.4 – 2.5 GHz [33].

Temperature distribution was solved by Penni's bioheat transfer equation, which mathematically models the physical heating phenomenon of the living tissues. This is the widely used model for heat interaction studies of human tissues [34-38] and is given by the following Equation 1.

$$\nabla \cdot (k\nabla T) + q_p + q_m - \omega c_b (T - T_a) = \rho c_p \frac{\partial T}{\partial t} \quad (1)$$

where $k$ is the thermal conductivity of tissue (W/m/°C); $T$ and $T_a$ is the local tissue temperature and arterial temperature in °C respectively; $q_p$ and $q_m$ is the energy deposition and metabolism rate (W/m$^3$) respectively; $\omega$ is the local blood perfusion rate (kg/m$^3$/s) of tissue; $c_b$ and $c_p$ are the specific heat (J/kg/°C) of blood and tissue material respectively; $\rho$ is the density (kg/m$^3$) of tissue material; and $t$ is the time (sec).

The EM wave interaction was solved by the vector-Helmholtz equation at the selected frequency, which is give as below by Equation 2.

$$\nabla \times \frac{1}{\mu_r} \nabla \times E - k_0^2 \varepsilon_r E = 0 \quad (2)$$

where E represents the field, $\mu_r$ is the relative permeability, $k_0$ is the wave vector in free-space and $\varepsilon_r$ represents the permittivity.

Finally, the specific absorption rate (SAR) is calculated which represents the RF energy absorbed by tissue in per unit time and is calculated from the tissue density and the electromagnetic dissipation density. This is important to estimate the usability of such setup from the safety point of view, which is done by comparing the maximum exposure values with the prescribed limits. It is estimated by applying the following Equation 3.

$$\text{SAR} = \sigma \frac{|E|^2}{\rho} \quad (3)$$

where $\sigma$ represents the tissues electric conductivity, $|E|$ is the electric field (RMS) norm, and $\rho$ is the tissue density. The SAR value is calculated herein in watts per kilogram (W/kg).

The finite element method (FEM) method is used to solve the governing partial differential equations (PDEs) which is formulated in COMSOL Multiphysics. The energy exchange between the metabolism and blood perfusion is been overlooked for future ex-vivo testing. The patch and phantom model were meshed with free tetrahedral form elements having 68574 degrees of freedom, while the remaining boundary regions were built with free triangular mesh.

## III. Results and Discussions

The average relative permittivity plot is more like a clarification that the model is properly generated and that the comparison models are properly correlated with the results. The mean relative permittivity (emw) contour graphs for all antenna designs are shown in Fig. 2 and were recreated using imported MRI image data [31] from which permittivity values are determined. The stroke is also seen here, showing the cross section of the stroke by taking the required reference plane.

The bioheat transfer study converts the incident waves into heat energy which is solved in the chosen COMSOL Multiphysics RF module. Based on the solutions derived from this analysis the temperature distribution plots are generated as shown by Fig. 3 (surface temperature plot which tells only the surface effect as the name suggests) and Fig. 4 (sub-surface temperature plot, which gives a detailed understanding of the induced heating). The noted surface temperature rise (°C) values due to the incident EM waves induced heating is 8.95 x $10^{-7}$, 4.45 x $10^{-7}$, 5.02 x $10^{-7}$, 14 x $10^{-7}$, and 5.41 x $10^{-7}$ for when the antenna-A, antenna-B, antenna-C, antenna-D, and antenna-E respectively are used. This implies that the antenna-D is creating more surface heating effects amongst all the designs. Considering the iso-surface heating effect due to the incident waves, the temperature rise (°C) values are 85.02 x $10^{-8}$, 42.34 x $10^{-8}$, 48.80 x $10^{-8}$, 133.92 x $10^{-8}$, and 51.39 x $10^{-8}$ for when the antenna-A, antenna-B, antenna-C, antenna-D, and antenna-E respectively are used. Again, here also the antenna-D stands out as the most heating type design. Though considering the absolute values of the temperature rise, the rise is still not very high to create an adverse effect.

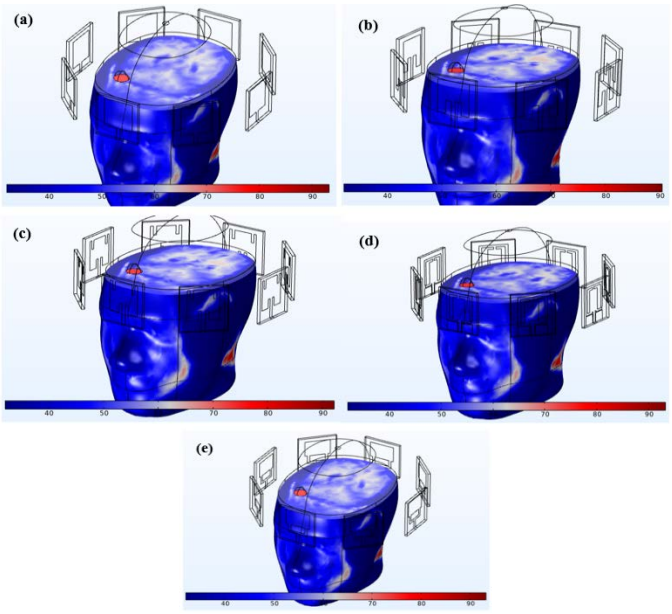


Fig. 2. The Average Relative Permittivity (emw) Contour Plots of the Stroke Containing Human Head Phantom under the Influence of Microwave Irradiation by Various Antenna Designs viz. (a) Antenna-A, (b) Antenna-B, (c) Antenna-C, (d) Antenna-D, and (e) Antenna-E.

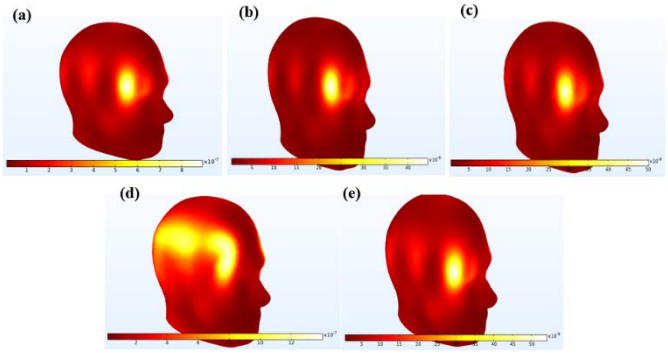


Fig. 3. Surface Temperature Plots of the Stroke Containing Human Head Phantom under the Influence of Microwave Irradiation by Various Antenna Designs viz. (a) Antenna-A, (b) Antenna-B, (c) Antenna-C, (d) Antenna-D, and (e) Antenna-E.

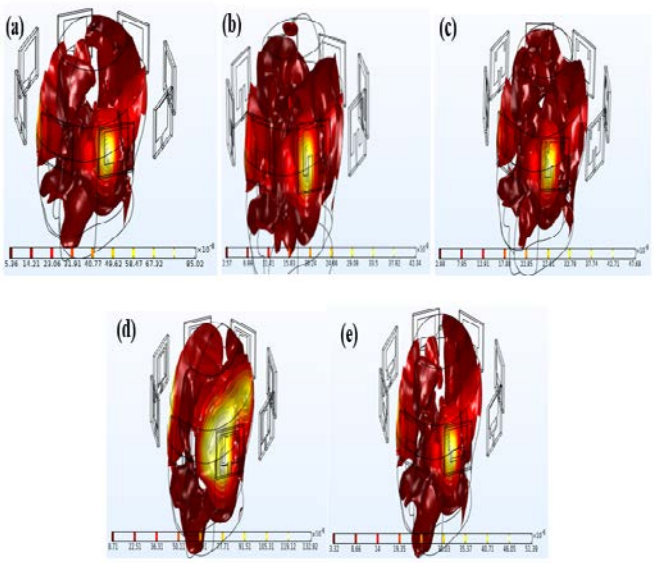


Fig. 4. Isothermal (Isosurface) Contours of the Stroke Containing Human Head Phantom under the Influence of Microwave Irradiation by Various Antenna Designs viz. (a) Antenna-A, (b) Antenna-B, (c) Antenna-C, (d) Antenna-D, and (e) Antenna-E.

The following results present the SAR rate by the head phantom due to the induced waves from the antenna array. The highest SAR value is observed near the regions of the phantom that are directly facing or nearby the antenna's incident electric field. Usually, the amount of SAR recorded depends on the number of antenna and their positioning & dielectric properties. The regions of the head phantom have distinct values of dielectric properties (permittivity and conductivity) which varies with the induced frequency and geometry of the antenna. Hence, the SAR which varies for the RF dependent human tissues; depends on the change in antenna design when the frequency is kept constant. This functionality is exploited for the key aspect of stroke identification since the blood clotted region responds differently than the surrounding tissue mass.

The simulated SAR fields on the human head phantom having the stroke, for the five antenna designs arranged in circumferential manner are shown in Fig. 5 (volumetric plot) and Fig. 6 (slices contour). By analysing each SAR slice individually, the exact shape and location of the stroke can be concluded. For example, the layered SAR slices (front view) arrangement is included in Section S2 in Supporting Information. The observation was carried out on the whole head phantom at 2.45 GHz. This arrangement of observation gives a unified way of locating the stroke position, both horizontally and vertically. This also benefits with the shape identification of the stroke for variable sizes, shapes, and positions. Higher SAR value hence is not desirable because it creates uneasiness and adverse health effects [39], also its increased value hints at higher resistive losses [40].

From all the result plots of the SAR exposure in W/g as shown in Fig. 7 the SAR value is higher near the antenna premises (near field area), where existence of strong electric field is obvious. The maximum SAR values (in W/kg) observed are $1.44 \times 10^{-5}$, $7.56 \times 10^{-6}$, $8.12 \times 10^{-6}$, $1.96 \times 10^{-5}$, and $8.63 \times 10^{-6}$ for when the antenna-A, antenna-B, antenna-C, antenna-D, and antenna-E respectively are used. All the observed values are quite lower than the described safety limit of 1.6 – 2 W/g for 1g of human tissue model [41].

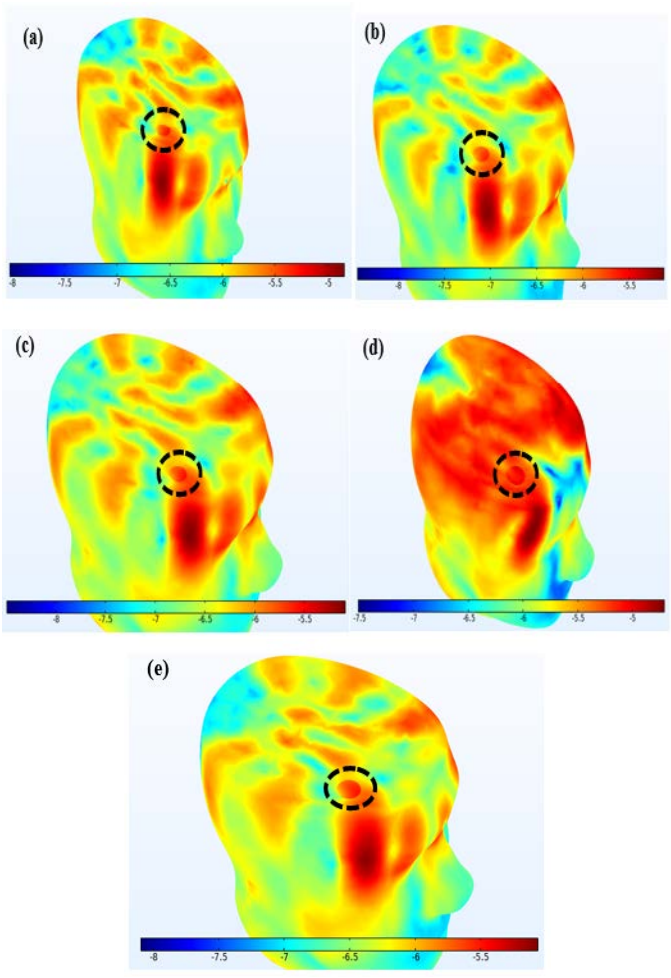


Fig. 5. Horizontal Cross-Sectional Layout of the SAR (Volumetric) Log-Scale Plot Showing the Exact Stroke Location in the Top view (the Exact Positioning of the Stroke Location in Horizontal Plane and its Shape is Indicated Herein) by various Antenna Designs viz. (a) Antenna-A, (b) Antenna-B, (c) Antenna-C, (d) Antenna-D, and (e) Antenna-E.

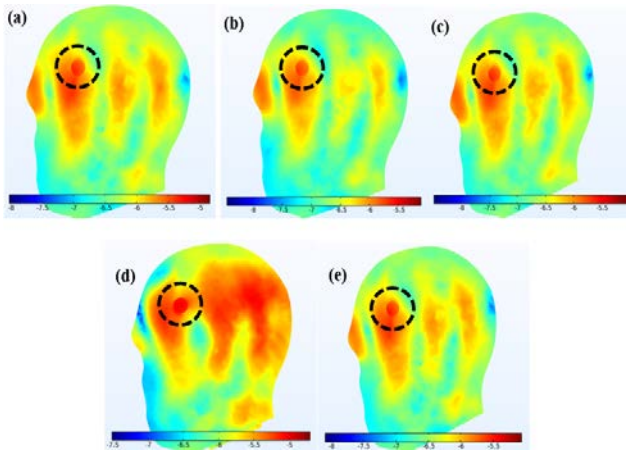


Fig. 6. Front view Layout of the Selected Local SAR Value Log-Scale Slice Plot showing the Exact Stroke Location (the Exact Positioning of the Stroke Location in Vertical Plane and its Shape is indicated herein) by various Antenna Designs viz. (a) Antenna-A, (b) Antenna-B, (c) Antenna-C, (d) Antenna-D, and (e) Antenna-E.

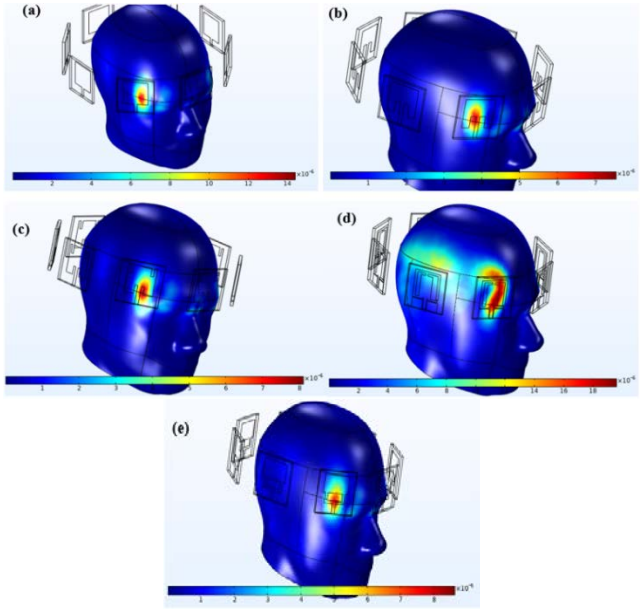


Fig. 7. Contour Plots representing Specific Absorption Rate in W/kg under the Influence of Microwave Irradiation by various Antenna Designs viz. (a) Antenna-A, (b) Antenna-B, (c) Antenna-C, (d) Antenna-D, and (e) Antenna-E.

The reduction in SAR values can be possibly due to two reasons viz. reduction of the input signal power or covering the antenna with the more dielectric material. By comparing the make designs of antenna-B, antenna-C, and antenna-E with antenna-A & antenna-D, the former one's had more dielectric material as the patch board. Hence, resulting in lower SAR values and making them a favorable choice of selection. Further, the antenna designs are also simulated to observe the effect on the reflection parameter/gain and the changes of SAR value with different designs. The investigated results are summarized for the reflection parameter and are separately discussed later in the last part of this section.

Fig. 8 shows the magnitude of the induced electric field within the head phantom with stroke included within, for all the antenna setups in terms of the x-component, y-component, and z-component. Herein the component of the electric field on the phantom surface is estimated and utilized for completing the imaging. The induced electric field values (emw) were 0.16, 0.1, 0.12, 0.25, and 0.13 for when the antenna-A, antenna-B, antenna-C, antenna-D, and antenna-E respectively are used for the stroke monitoring. The higher induced field implies that the details of the anatomical significance can be captured rapidly and with finer details, with measurement possible for minutely detailed examinations [42]. Hence, from this result, it comes out that the antenna-D should be the most desirable choice.

The performance comparison of the various antenna designs can be done by analyzing the 2-D far-field radiation patterns as shown in Fig. 9. This is a plot of the far-field norm represented in V/m. The 8x8 patch antenna array gain pattern (red) for all antennas show the main lobe and even the directional side lobes, but the main thing observed is that the emerging side lobes at 45° towards the right are more prominent and hence will dictate the direction of propagation. Though the 45° prominent lobes also signify that more area can be covered by the antenna designs. Considering the single patch antenna gain plot (blue), the pattern is similar for the antenna-B, antenna-C, and antenna-E; but for the antenna-A and antenna-D they have a distinctive bulging shape. The antenna-A shows very big area of the plot as compared to all others, representing that it can generate the wave with the most power, but it lacks directional streamlining. Hence, considering the directional antenna traits, other antenna designs will perform better.

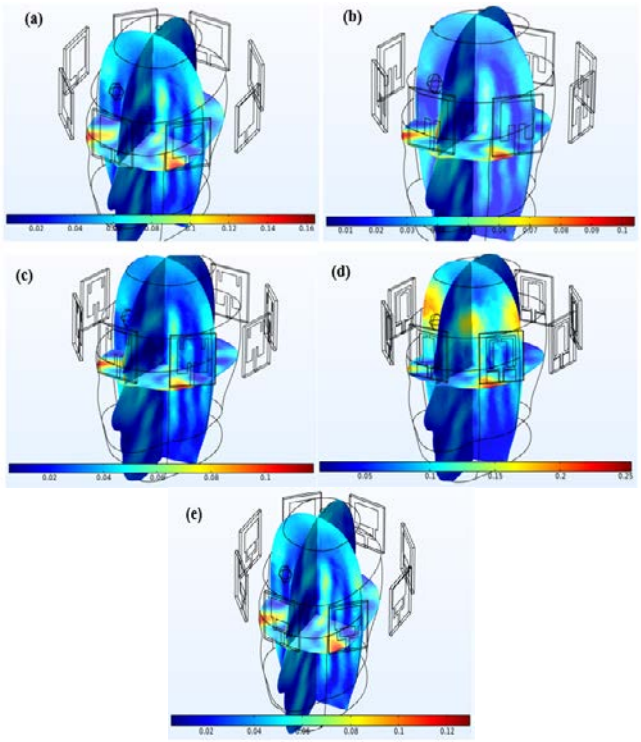


Fig. 8. The Induced Electric Field (emw) in the Stroke Containing Human Head Phantom under the Influence of Microwave Irradiation by various Antenna Designs viz. (a) Antenna-A, (b) Antenna-B, (c) Antenna-C, (d) Antenna-D, and (e) Antenna-E.

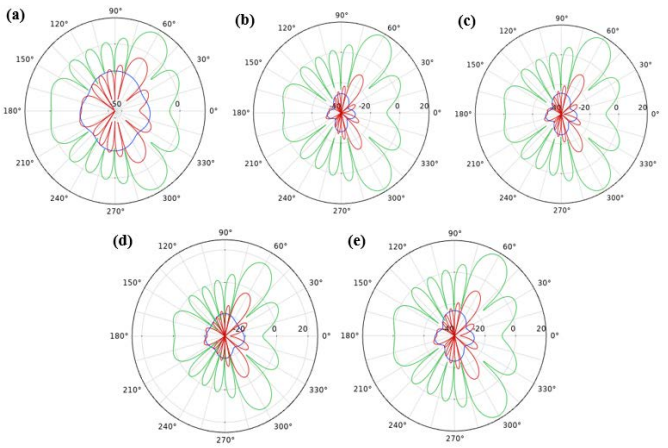


Fig. 9. 2-D Far-Field Radiation Patterns for the various Antenna Designs Studied in this Simulation Study viz. (a) Antenna-A, (b) Antenna-B, (c) Antenna-C, (d) Antenna-D, and (e) Antenna-E. Wherein, the Blue, Green and Red Trajectories represent Single Patch Antenna Gain, 8x8 uniform Array Factor, and 8x8 Patch Antenna Array Gain respectively.

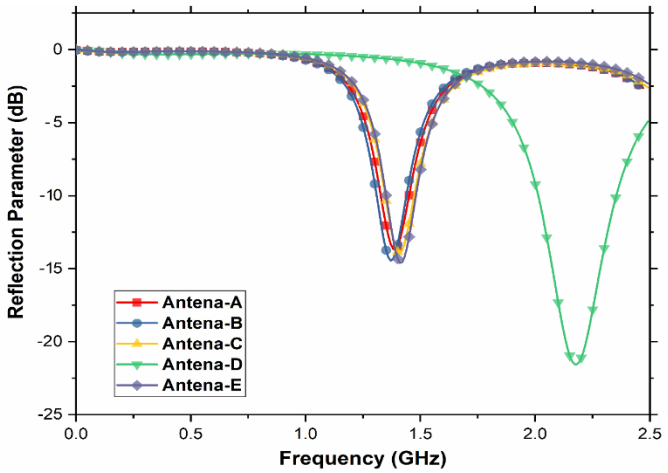


Fig. 10. Reflection Parameter (S11) Comparison Plot for all the Antenna Designs studied herein.

The reflection parameters also commonly known as reflection loss or simply S11 values; were calculated by frequency sweep in the range between 0 – 2.5 GHz for the five types of antennas and the comparison plot is shown in Fig. 10. All the values are lower than 0 dB (negative range) in the studied frequency range, which suggests that the antennas can operate efficiently when mounted on the head phantom [43]. The antennas A, B, C and E showed almost similar performance, with resonances around 1.3 - 1.5 GHz; the antenna D design, shows an S11 value under −22 dB for frequencies above 2.2 GHz. The antenna D operates more efficiently above 1.5 GHz, with a deep resonance around 2.2 GHz, making it ideal for the studied application in this research for stroke detection at the medically prescribed frequency level of 2.4 – 2.5 GHz.

## IV. Conclusions

In this study, the concept of stroke identification and location is presented along with the analysis of the most suitable antenna design to be used, amongst the five chosen designs. The simulation study for the stroke identification with the five chosen antenna designs was successfully presented at 2.45 GHz frequency; as a means for addressing the queries related to the suitable antenna selection for the future experimental study. The results from the bioheat transfer module gave a clear understanding of the surface and sub-surface temperature rise due to the induced field, suggesting that the antenna-D had the highest sub-surface rise of 133.92 x $10^{-8}$ °C. But the main purpose of identifying the stroke presence with its shape, size, and location was accomplished by the SAR modeling for all the antenna design cases, by analyzing the appropriate horizontal and vertical SAR slices. Furthermore, the key concern of reducing the SAR for presenting the possibility of multiple usages without harmful effects unlike ionizing radiations was achieved with the antenna-A and antenna-D designs likewise. Overall, considering all the results discussed the antenna-D can be considered as the most suitable choice for future experimental prototyping and proving the efficacy of this concept. Based on this the experimental testing will be following as the next study.

## Acknowledgment

The preferred work was supported by the Deanship of Scientific Research at Majmaah University under Project No. RGP- 2019-32.

## References

[1] World Health Organization Global health estimates: deaths by cause, age, sex and country, 2000-2012. Geneva, WHO 2014, 9.

[2] Owolabi, M.O.; Akarolo-Anthony, S.; Akinyemi, R.; Arnett, D.; Gebregziabher, M.; Jenkins, C.; Tiwari, H.; Arulogun, O.; Akpalu, A.; Sarfo, F.S.; Obiako, R.; Owolabi, L.; Sagoe, K.; Melikam, S.; Adeoye, A.M.; Lackland, D.; Ovbiagele, B.; Members of the H3Africa Consortium The burden of stroke in Africa: a glance at the present and a glimpse into the future. Cardiovasc J Afr 2015, 26, S27-38.

[3] Johnson, W.; Onuma, O.; Owolabi, M.; Sachdev, S. Stroke: a global response is needed. Bull World Health Organ 2016, 94, 634-634A.

[4] Feigin, V.L.; Forouzanfar, M.H.; Krishnamurthi, R.; Mensah, G.A.; Connor, M.; Bennett, D.A.; Moran, A.E.; Sacco, R.L.; Anderson, L.; Truelsen, T.; O'Donnell, M.; Venketasubramanian, N.; Barker-Collo, S.; Lawes, C.M.; Wang, W.; Shinohara, Y.; Witt, E.; Ezzati, M.; Naghavi, M.; Murray, C.; Global Burden of Diseases, Injuries, and Risk Factors Study 2010 (GBD 2010) and the GBD Stroke Experts Group Global and regional burden of stroke during 1990-2010: findings from the Global Burden of Disease Study 2010. Lancet 2014, 383, 245-254.

[5] Strong, K.; Mathers, C.; Bonita, R. Preventing stroke: saving lives around the world. The Lancet Neurology 2007, 6, 182-187.

[6] Chandra, R.; Zhou, H.; Balasingham, I.; Narayanan, R.M. On the opportunities and challenges in microwave medical sensing and imaging. IEEE transactions on biomedical engineering 2015, 62, 1667-1682.

[7] Walsh, K.B. Non-invasive sensor Technology for Prehospital Stroke Diagnosis: current status and future directions. International Journal of Stroke 2019, 14, 592-602.

[8] Shao, Y.; Tsai, K.; Kim, S.; Wu, Y.; Demissie, K. Exposure to Tomographic Scans and Cancer Risks. JNCI Cancer Spectrum 2020, 4, pkz072.

[9] Mayosi, B.M.; Lawn, J.E.; Van Niekerk, A.; Bradshaw, D.; Karim, S.S.A.; Coovadia, H.M.; Lancet South Africa team Health in South Africa: changes and challenges since 2009. The Lancet 2012, 380, 2029-2043.

[10] O'donnell, M.J.; Xavier, D.; Liu, L.; Zhang, H.; Chin, S.L.; Rao-Melacini, P.; Rangarajan, S.; Islam, S.; Pais, P.; McQueen, M.J. Risk factors for ischaemic and intracerebral haemorrhagic stroke in 22

countries (the INTERSTROKE study): a case-control study. The Lancet 2010, 376, 112-123.

[11] A. Zamani, A. M. Abbosh, and A. T. Mobashsher, "Fast frequency-based multistatic microwave imaging algorithm with application to brain injury detection," IEEE Trans. Microw. Theory Techn., vol. 64, no. 2, pp. 653– 662, Feb. 2016.

[12] Walsh, K.B. Non-invasive sensor Technology for Prehospital Stroke Diagnosis: current status and future directions. International Journal of Stroke 2019, 14, 592-602.

[13] Mobashsher, A.T.; Bialkowski, K.; Abbosh, A.; Crozier, S. Design and experimental evaluation of a non-invasive microwave head imaging system for intracranial haemorrhage detection. Plos one 2016, 11, e0152351.

[14] Merunka, I.; Massa, A.; Vrba, D.; Fiser, O.; Salucci, M.; Vrba, J. Microwave tomography system for methodical testing of human brain stroke detection approaches. International Journal of Antennas and Propagation 2019.

[15] Fhager, A.; Candefjord, S.; Elam, M.; Persson, M. Microwave diagnostics ahead: Saving time and the lives of trauma and stroke patients. IEEE Microwave Magazine 2018, 19, 78-90.

[16] Karadima, O.; Rahman, M.; Sotiriou, I.; Ghavami, N.; Lu, P.; Ahsan, S.; Kosmas, P. Experimental Validation of Microwave Tomography with the DBIM-TwIST Algorithm for Brain Stroke Detection and Classification. Sensors 2020, 20, 840.

[17] Mobashsher, A.T.; Abbosh, A. On-site rapid diagnosis of intracranial hematoma using portable multi-slice microwave imaging system. Scientific reports 2016, 6, 37620.

[18] Hopfer, M.; Planas, R.; Hamidipour, A.; Henriksson, T.; Semenov, S. Electromagnetic Tomography for Detection, Differentiation, and Monitoring of Brain Stroke: A Virtual Data and Human Head Phantom Study. IEEE Antennas and Propagation Magazine 2017, 59, 86-97.

[19] Bisio, I.; Fedeli, A.; Lavagetto, F.; Pastorino, M.; Randazzo, A.; Sciarrone, A.; Tavanti, E. A numerical study concerning brain stroke detection by microwave imaging systems. Multimedia Tools Appl 2018, 77, 9341-9363.

[20] Alqadami, A.S.; Bialkowski, K.S.; Mobashsher, A.T.; Abbosh, A.M. Wearable electromagnetic head imaging system using flexible wideband antenna array based on polymer technology for brain stroke diagnosis. IEEE transactions on biomedical circuits and systems 2018, 13, 124-134.

[21] Afsari, A.; Abbosh, A.M.; Rahmat-Samii, Y. Modified born iterative method in medical electromagnetic tomography using magnetic field fluctuation contrast source operator. IEEE Trans Microwave Theory Tech 2018, 67, 454-463.

[22] Maffongelli, M.; Poretti, S.; Salvadè, A.; Monleone, R.; Pagnamenta, C.; Fedeli, A.; Pastorino, M.; Randazzo, A. Design and experimental test of a microwave system for quantitative biomedical imaging, 2018 IEEE International Symposium on Medical Measurements and Applications (MeMeA), IEEE: 2018; , pp. 1-6.

[23] Persson, M.; Fhager, A.; Trefná, H.D.; Yu, Y.; McKelvey, T.; Pegenius, G.; Karlsson, J.; Elam, M. Microwave-based stroke diagnosis making global prehospital thrombolytic treatment possible. IEEE Transactions on Biomedical Engineering 2014, 61, 2806-2817.

[24] Candefjord, S.; Winges, J.; Malik, A.A.; Yu, Y.; Rylander, T.; McKelvey, T.; Fhager, A.; Elam, M.; Persson, M. Microwave technology for detecting traumatic intracranial bleedings: tests on phantom of subdural hematoma and numerical simulations. Med Biol Eng Comput 2017, 55, 1177-1188.

[25] D. Ireland, K. Bialkowski, and A. Abbosh, "Microwave imaging for brain stroke detection using Born iterative method," IET Microw. Antennas Propag., vol. 7, no. 11, pp. 909–915, Aug. 2013.

[26] IEEE Standards Coordinating Committee 34 IEEE Recommended Practice for Determining the Peak Spatial-average Specific Absorption Rate (SAR) in the Human Head from Wireless Communications Devices: Measurement Techniques, Institute of Electrical and Electronic Engineers: 2003.

[27] IEC 62209–1 Human exposure to radio frequency fields from hand-held and body-mounted wireless communication devices—Human models, instrumentation, and procedures—Part 1: Procedure to determine the specific absorption rate (SAR) for hand-held devices used in close proximity to the ear (frequency range of 300 MHz to 3 GHz). 2005.

[28] ARIB, S. Specific absorption rate (SAR) estimation for cellular phone. ARIB STD-T56 1998.

[29] ENS, C.S. 50361:"Basic Standard for the measurement of Specific Absorption Rate related to human exposure to electromagnetic fields from mobile phones (300 MHz-3 GHz),". Brussels, Belgium, CENELEC 2001.

[30] Fields, R.E. Evaluating compliance with FCC guidelines for human exposure to radiofrequency electromagnetic fields. OET bulletin 1997,

[31] Levoy, M. The Stanford volume data archive. URL: http://graphics.stanford.edu/data/voldata 2001.

[32] Schmid, G.; Neubauer, G.; Mazal, P.R. Dielectric properties of human brain tissue measured less than 10 h postmortem at frequencies from 800 to 2450 MHz. Bioelectromagnetics: Journal of the Bioelectromagnetics Society, The Society for Physical Regulation in Biology and Medicine, The European Bioelectromagnetics Association 2003, 24, 423-430.

[33] Yang, Z.; Xiao, S.; Zhu, L.; Wang, B.; Tu, H. A circularly polarized implantable antenna for 2.4-GHz ISM band biomedical applications. IEEE Antennas and Wireless Propagation Letters 2017, 16, 2554-2557.

[34] Chen, M.M.; Holmes, K.R. Microvascular contributions in tissue heat transfer. Ann N Y Acad Sci 1980, 335, 137-150.

[35] Weinbaum, S.; Jiji, L. A new simplified bioheat equation for the effect of blood flow on local average tissue temperature. 1985.

[36] Baish, J.; Ayyaswamy, P.; Foster, K. Small-scale temperature fluctuations in perfused tissue during local hyperthermia. 1986.

[37] Perez, F.P.; Bandeira, J.P.; Morisaki, J.J.; Krishna Peddinti, S.V.; Salama, P.; Rizkalla, J.; Rizkalla, M.E. Antenna Design and SAR Analysis on Human Head Phantom Simulation for Future Clinical Applications. J Biomed Sci Eng 2017, 10, 421-430.

[38] Shih, T.; Yuan, P.; Lin, W.; Kou, H. Analytical analysis of the Pennes bioheat transfer equation with sinusoidal heat flux condition on skin surface. Med Eng Phys 2007, 29, 946-953.

[39] Bond, S.; Wang, K. The Impact of Cell Phone Towers on House Prices in Residential Neighborhoods. Appraisal J 2005, 73.

[40] El-Sharkawy, A.M.; Qian, D.; Bottomley, P.A.; Edelstein, W.A. A multichannel, real-time MRI RF power monitor for independent SAR determination. Med Phys 2012, 39, 2334-2341.

[41] Lin, J.C. A new IEEE standard for safety levels with respect to human exposure to radio-frequency radiation. IEEE Antennas and Propagation Magazine 2006, 48, 157-159.

[42] Qureshi, A.M.; Mustansar, Z. Levels of detail analysis of microwave scattering from human head models for brain stroke detection. PeerJ 2017, 5, e4061.

[43] Guo, W.; Ahsan, S.; He, M.; Koutsoupidou, M.; Kosmas, P. Printed monopole antenna designs for a microwave head scanner, 2018 18th Mediterranean Microwave Symposium (MMS), IEEE: 2018; , pp. 384-386